



Phase-conjugate mirror for water waves driven by the Faraday instability

Vincent Bacot^{a,1}, Guillaume Durey^{a,1}, Antonin Eddi^b, Mathias Fink^a, and Emmanuel Fort^{a,2}

^aInstitut Langevin, ESPCI Paris, PSL University, CNRS, 75005 Paris, France; and ^bPhysique et Mécanique des Milieux Hétérogènes, ESPCI Paris, PSL University, CNRS, Sorbonne Université, Université Paris Diderot, Sorbonne Paris Cité, 75005 Paris, France

Edited by David A. Weitz, Harvard University, Cambridge, MA, and approved March 25, 2019 (received for review December 3, 2018)

The Faraday instability appears on liquid baths submitted to vertical oscillations above a critical value. The pattern of standing ripples at half the vibrating frequency that results from this parametric forcing is usually shaped by the boundary conditions imposed by the enclosing receptacle. Here, we show that the time modulation of the medium involved in the Faraday instability can act as a phase-conjugate mirror—a fact which is hidden in the extensively studied case of the boundary-driven regime. We first demonstrate the complete analogy with the equations governing its optical counterpart. We then use water baths combining shallow and deep areas of arbitrary shapes to spatially localize the Faraday instability. We give experimental evidence of the ability of the Faraday instability to generate counterpropagating phase-conjugated waves for any propagating signal wave. The canonical geometries of a point and plane source are implemented. We also verify that Faraday-based phase-conjugate mirrors hold the genuine property of being shape independent. These results show that a periodic modulation of the effective gravity can perform time-reversal operations on monochromatic propagating water waves, with a remarkable efficiency compared with wave manipulation in other fields of physics.

phase-conjugate mirror | Faraday instability | wave control | water wave

In 1831, Faraday discovered that submitting a bath to a periodic vertical acceleration resulted in the destabilization of its surface above an acceleration threshold (1). This parametric instability, known as the Faraday instability, is driven by the modulation of the effective gravity. Surface waves appear as standing waves, modulated at half the excitation frequency. This instability has been extensively studied, both experimentally and theoretically, in the steady-state regime (2–4). In this regime, the wave pattern is dominated by the geometry of the bath, the boundaries and menisci acting as wave sources. The observed wave field is thus a combination of some modes of the cavity defined by the shape of the bath (2). The extended literature on the Faraday instability has focused on aspects like the nonlinear hydrodynamic regimes (5, 6), the influence of the depth or of the viscosity of the liquid (7, 8), the excitation under several frequencies (7, 9), or the ability to generate droplets (10, 11). However, all these studies only consider the steady-state regime with standing-wave patterns, after the transient growth of the instability, and no external wave input.

This is in stark contrast with nonlinear (NL) optics, in which parametric forcing has been very fruitful to master optical beams. In particular, this has enabled the design of phase-conjugate mirrors (12–14) (PCMs). Typically, a monochromatic wave field with an arbitrary shape enters the NL optical crystal and generates a counterpropagating, time-reversed wave field. In the four-wave mixing (FWM) implementation, the parametric modulation is provided by two external pump beams (13).

On the contrary, in fluid mechanics, the Faraday instability has always been analyzed within the framework of parametric instabilities, thus ignoring its additional ability to control and manipulate propagating waves. In this paper, we revisit it as a means to perform phase conjugation on water waves, through a periodic time modulation of the medium properties. We show that it does act as a PCM for water waves at the Faraday frequency.

The paper is organized as follows. In the first section, we show the formal analogy between the Faraday instability and an optical PCM obtained by an FWM configuration in an NL optical material. Section 2 is devoted to the description of the experimental implementation, in which the water-wave PCM is confined to a specific area in the bath, taking advantage of the Faraday threshold dependence on the liquid depth. Section 3 presents and discusses the experimental results for standard point and plane source geometries. In addition, using arbitrary mirror shapes, we show that PCM refocusing is independent of the geometry of the mirror.

Theoretical Developments

In this section, we provide evidence for the analogy between the Faraday instability and an optical PCM produced by NL optics. In optics, one of the most common ways to achieve phase conjugation is through the backward degenerate FWM configuration, first proposed by Hellwarth in 1977 (12). A schematic of the configuration is shown in Fig. 1A. When a monochromatic point source emits a wave into the NL optical crystal, the PCM generates a counterpropagating wave which refocuses at the source position. This clearly shows that a PCM acts as a monochromatic time-reversal mirror. Note also that contrary to standard mirrors, this is independent of the shape of the crystal. It is based on the third-order susceptibility $\chi^{(3)}$ of an NL optical medium. Two counterpropagating, high-intensity plane waves, called pump waves, are sent on the NL medium. Neglecting the vector nature of the fields, their associated electric fields are given by $E_1 = A_p e^{i(\omega t - k_p \cdot r)}$ and $E_2 = A_p e^{i(\omega t + k_p \cdot r)}$, respectively, where ω is the time angular frequency, k_p the wave vector, and A_p the wave

Significance

Nonlinear and parametric processes are central in mastering wave propagation. They are at the core of numerous applications in optics and acoustics. In the case of water waves, the Faraday instability is the archetype of a parametric excitation. A periodic vertical excitation results in the destabilization of a liquid interface. However, it has always been interpreted as an instability, completely overshadowing its potential to control water-wave propagation. In this paper, we unveil the ability of this temporal modulation to act as a phase-conjugate mirror. We show that waves refocus to any initial emitting source position, whatever the shape of the mirror. This paper thus revisits this historical instability and opens up exciting perspectives in water-wave manipulation.

Author contributions: V.B., G.D., A.E., M.F., and E.F. designed research; V.B., G.D., and E.F. performed research; V.B., G.D., A.E., and E.F. analyzed data; and V.B., G.D., A.E., M.F., and E.F. wrote the paper.

The authors declare no conflict of interest.

This article is a PNAS Direct Submission.

Published under the PNAS license.

¹V.B. and G.D. contributed equally to this work.

²To whom correspondence should be addressed. Email: emmanuel.fort@espci.fr.

This article contains supporting information online at www.pnas.org/lookup/suppl/doi:10.1073/pnas.1818742116/-DCSupplemental.

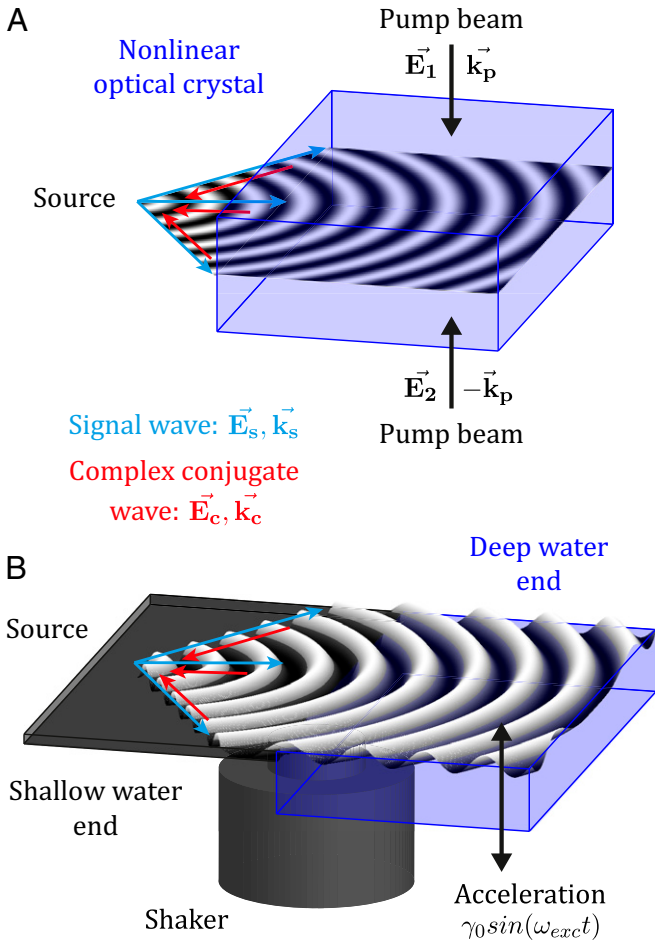


Fig. 1. Schematics of phase-conjugate mirrors for optics and water waves. (A) Optical implementation of a PCM with an NL optical crystal using the four-wave mixing configuration, with two counterpropagating pump beams orthogonal to the signal wave emitted from a point source. A conjugated wave is generated in the crystal by the time modulation of the refractive index induced by the interference of the pumps. (B) Water-wave implementation of the PCM in the same configuration. The bath is submitted to a sinusoidal vertical acceleration to modulate the wave-propagation speed in time. The dependence of the Faraday instability threshold on the water depth is used to obtain the analog of the free propagation and propagation in the optical NL crystal, using a shallow- and a deep-water bath, respectively.

amplitude. When a signal wave $E_s = A_s e^{i(\omega t - \mathbf{k}_s \cdot \mathbf{r})}$ with the same angular frequency ω and a wave vector \mathbf{k}_s is sent into the NL medium, it generates a counterpropagating idler wave $E_c = A_c e^{i(\omega t - \mathbf{k}_c \cdot \mathbf{r})}$ with the same angular frequency ω and a wave vector \mathbf{k}_c equal to $-\mathbf{k}_s$. Under the usual assumptions that the high-intensity pump waves are not depleted by the (weak) NL interaction and remain constant (14), the signal and the idler modes $E_{s/c}$ are coupled, and can be expressed as a set of coupled equations in the presence of the NL polarization:

$$\Delta E_{s/c} - \frac{n_{\text{eff}}^2}{c^2} \frac{\partial^2 E_{s/c}}{\partial t^2} = -\frac{6\omega^2 \chi^{(3)} A_p^2}{c^2} e^{2i\omega t} E_{c/s}^* \quad [1]$$

where $n_{\text{eff}}^2 = 1 + 6\chi^{(3)} |A_p|^2$. The two modes E_s and E_c are the phase conjugates of each other: They are coupled by sources proportional to their complex conjugate (right-hand side of the equation). This is equivalent to time reversal for monochromatic waves. The real electric field of the idler mode $\mathcal{E}_c(\mathbf{r}, t)$ at time t satisfies

$$\mathcal{E}_c(\mathbf{r}, t) = \text{Re} \left[A_c e^{i(\omega t - \mathbf{k}_c \cdot \mathbf{r})} \right] \propto \text{Re} \left[A_s^* e^{i(-\omega t + \mathbf{k}_s \cdot \mathbf{r})} \right] = \mathcal{E}_s(\mathbf{r}, -t), \quad [2]$$

where $\mathcal{E}_s(\mathbf{r}, -t)$ is the real electric field associated with the signal mode at time $-t$. Note that the effect of the pump waves is equivalent to a temporal modulation of the refractive index with the doubled frequency (14):

$$n_{\text{mod}}^2 = n_{\text{eff}}^2 + 6\chi^{(3)} A_p^2 e^{2i\omega t}. \quad [3]$$

Let us now show that these equations are formally analogous to the ones which describe the propagation of water waves on a vibrated bath with a temporal angular frequency $\omega_{\text{exc}} = 2\omega$. In the deep-water regime (where the liquid depth verifies $h \gg \lambda$), neglecting viscosity, the equation for the free surface elevation field ζ can be written in the spatial Fourier space in the form of a Mathieu equation (2, 15):

$$\frac{\partial^2 \tilde{\zeta}(\mathbf{k}, t)}{\partial t^2} + \omega_0^2(k) \tilde{\zeta}(\mathbf{k}, t) = -\gamma_0 k \cos(2\omega t) \tilde{\zeta}(\mathbf{k}, t), \quad [4]$$

with $k = |\mathbf{k}|$ the norm of the wave vector, and $\omega_0(k)$ the time angular frequency satisfying the dispersion relation of linear gravito-capillary waves $\omega_0(k) = \sqrt{gk + (\sigma_S/\rho)k^3}$, g being the gravity acceleration, σ_S the surface tension, and ρ the density of the liquid. γ_0 is the amplitude of the acceleration of the bath vibrated at the angular frequency $\omega_{\text{exc}} = 2\omega$. In the general case, Floquet analysis shows that the solutions of Eq. 4 are of the form $e^{\mu t} f_{2\omega}(t)$, where μ is a complex number and $f_{2\omega}(t)$ is a periodic function at the angular frequency 2ω . Only the unstable modes corresponding to $\text{Re}[\mu] > 0$ are amplified (4). In the weak excitation limit ($\gamma_0 k \ll \omega^2$) valid in our experiments, it can be shown that these unstable modes must satisfy the dispersion relation of free surface waves, with frequencies selected by multiples of half the bath vibration frequency: $\omega(k_n) = n\omega$, where n is an integer. Let us assume that in such a modulated bath, a signal plane wave $\zeta_s = A_s e^{i(\omega t - \mathbf{k}_s \cdot \mathbf{r})}$ of frequency ω and of wave vector \mathbf{k}_s is introduced. Its spatial Fourier transform is $\tilde{\zeta}_s = A_s e^{i\omega t} \delta(\mathbf{k} - \mathbf{k}_s)$. Due to the modulation of the bath, other frequency components of the wave field may emerge. However, in the weak excitation limit, only the components of frequency ω are generated (2), so that we can assume that the Fourier transform of the total wave field can be written: $\tilde{\zeta} = \tilde{\zeta}_s + \tilde{\zeta}_c$, where $\tilde{\zeta}_c = A_c e^{-i\omega t} \delta(\mathbf{k} - \mathbf{k}_s)$. A_s and A_c are slowly varying envelopes compared with $1/\omega$ in the weak approximation limit. Eq. 4 can therefore be decomposed into a set of coupled equations for the components at angular frequency ω and $-\omega$:

$$\frac{\partial^2 \tilde{\zeta}_{s/c}}{\partial t^2} + \omega^2 \tilde{\zeta}_{s/c} = -\gamma_0 k e^{\pm 2i\omega t} \tilde{\zeta}_{c/s}^* \quad [5]$$

These coupled equations are identical to the coupled Eq. 1 describing the PCM in optics, the change of sign of the angular frequency being equivalent to a change of sign of the wave vector. Thus, the Faraday instability can be interpreted as a PCM for surface waves. Note that the formal analogy with optical PCMs predicts that the initial and the phase-conjugated waves converge to the same amplitude at large times (14). This is why the modulation of the medium and thus the Faraday instability are associated with standing waves in the long run. In the next section, we give experimental evidence of this interpretation of the Faraday instability.

Experimental Setup and Procedures

Fig. 1B shows a schematic of the water-wave analogous configuration using the Faraday instability. The role of the counterpropagating vertical optical pumps is played by the vertical vibration of the bath. Since the Faraday threshold strongly depends on the

depth of the liquid (16), we use the bathymetry (underwater topography) to split the bath into distinct areas mimicking the wave propagation in free space or in the optical NL crystal. In the shallow region, the excitation acceleration is far from the threshold, hence the vertical vibration has only negligible effects on the wave propagation: it appears similar to that of an unperturbed bath. In the deep-water region, the vertical acceleration is set slightly above the Faraday threshold. In this region, any propagating wave triggers a counterpropagating wave.

The experimental setup is shown in Fig. 2A. A $25 \times 25 \text{ cm}^2$ square container (made of polylactic acid with a 3D printer) is set on a vertically vibrating shaker (B&K Vibration Exciter type 4808, controlled by means of a waveform generator). The bath is divided in two adjacent rectangular areas with different depths: the shallow and deep ends are, respectively, $h_{<} = 0.5 \text{ mm}$ and $h_{>} = 6 \text{ mm}$ deep. The sinusoidal vertical acceleration satisfies $\gamma(t) = \gamma_0 H(t) \sin(2\pi f_{\text{exc}} t)$, with the frequency f_{exc} set to 35 Hz, and $H(t)$ the Heaviside step function. The walls of the bath are tilted 30° from the vertical direction, to limit the excitation of waves at the excitation frequency ω_{exc} by the menisci at the boundaries. Care is taken that the water wets the slope on each side.

The wave source is obtained using a loudspeaker operated by a second waveform generator. The loudspeaker produces variations of pressure in a hermetic cavity equipped with plastic tubing. Depending on the type of geometry needed for the wave source, the tubing can be plugged on various systems attached to the water container: A straw, whose tip is placed above the shallow end of the pool, at a distance of 2 cm ahead of the boundary with the deep end, is used as a point source; a flared hollow solid, with a series of 1-mm holes arranged in a line with a 3-mm spacing, is used as a planar source. An intense LED light (Constellation 60) is placed approximately 1 mm above the bath. A sheet of diffusing paper, on which a radial Gaussian filter is

printed, is positioned under the source to create a gradient in the illumination light. A semireflecting mirror is used to redirect the light reflected by the waves toward the camera, which records movies at 500 frames per second.

As shown in Fig. 2B, for a given acceleration γ_0 above the Faraday instability threshold γ_F in the deep end, the instability grows exponentially with a typical time τ_F , which depends on the distance to the threshold. This time is evaluated through the monitoring of σ , the variance of the intensity of the camera pixels imaging the deep end of the pool. Initially, the surface of the water is flat; σ is close to zero. At time $t=0$ the vertical vibration is turned on. The menisci at the boundaries of the bath act as a source of propagating ripples at the excitation frequency, hence σ increases to a small value. In the absence of a source signal, this noise triggers a pattern of standing waves at the Faraday frequency which starts building up in the deep end of the pool (Fig. 2B, *Inset*). This results in a sharp increase of σ . This instant defines τ_F , which is typically on the order of 10 s. Once the instability is fully established, the waves reach their maximum amplitude and σ reaches a plateau.

To produce a signal wave, the loudspeaker is sent 10 periods of a sinusoid at the Faraday frequency $f = 17.5 \text{ Hz}$, over a duration T_S . Fig. 2C shows a top view of the bath during the emission of a signal wave from a point source. Fig. 2D shows the space-time plot of the wave emission by the point source, taken along the x axis (red line in Fig. 2C). The signature of the outward-propagating nature of the waves is readily observed in the wave-front orientation. It takes a time Δt_p for the waves to reach the deep end and cross it. Fig. 2C and D was produced in the absence of a vertical excitation of the bath.

A typical experiment combines the vertical vibration with the production of a signal wave. It is crucial in these experiments that the Faraday instability be triggered in the deep end by the signal

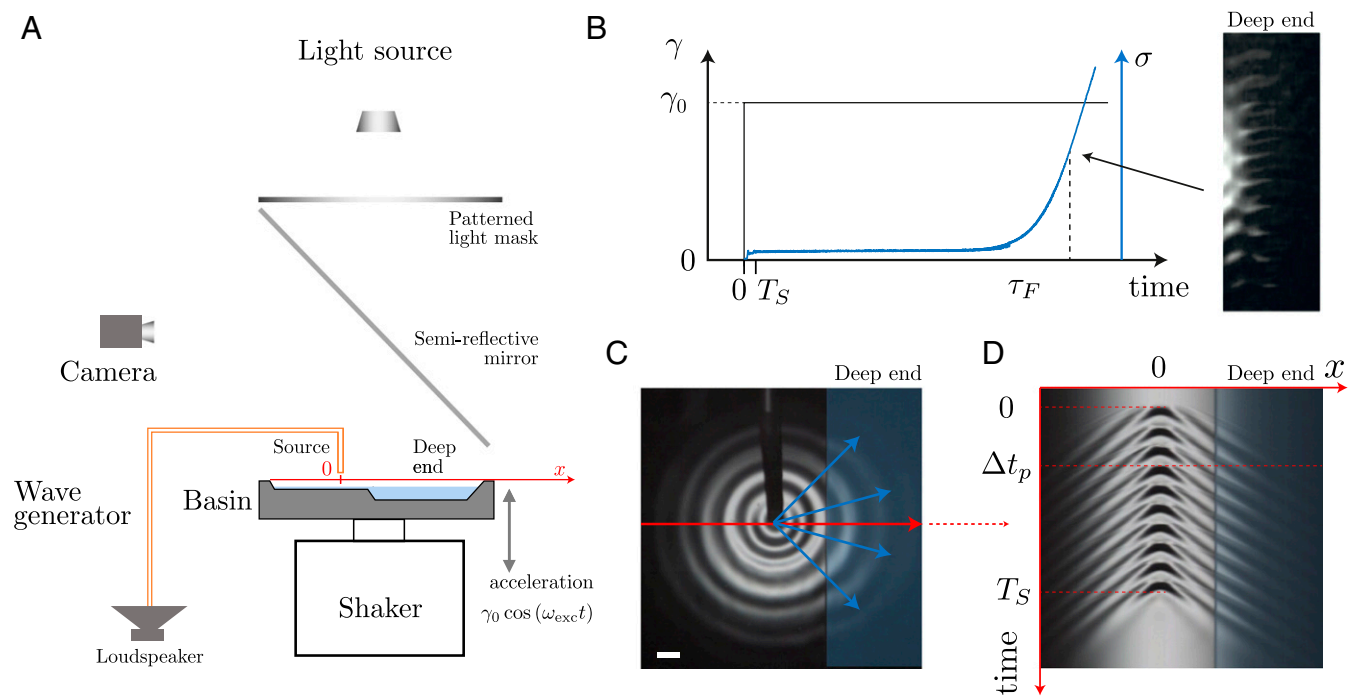


Fig. 2. Setup and experimental procedures. (A) Schematics of the experimental setup. (B) Temporal evolution of the amplitude of the acceleration γ_0 (black, left axis) and of the normalized SD σ of the intensity of the pixels in images of the deep end of the pool (blue, right axis). The origin of time is taken when the vibration is turned on. This gives the characteristic exponential growth time for the Faraday instability τ_F before saturation. (*Inset*) Snapshot of the growing Faraday instability. (C) Top view of the diverging waves on a still bath produced by the point source inducing a pressure oscillation at the Faraday frequency $f = 17.5 \text{ Hz}$. (D) Associated space-time plot along the line represented in C in red (x axis). Δt_p is the time taken by the emitted wave to reach the wall after crossing the deep end of the bath and T_S is the emission duration.

wave and not by the fluctuations of the bath or by the boundary-induced ripples. Thus, the time sequences are set so that $T_s + \Delta t_p \ll \tau_F$. This is possible since τ_F is typically on the order of 10 s, while $T_s + \Delta t_p$ is less than 1 s.

Despite the precautions taken to physically attenuate them, the boundaries of the bath emit small ripples throughout our experiments. Although they neither interfere with nor prevent the observation of the waves generated by the PCM, these ripples were removed numerically to improve the aesthetic appearance of the movies. Since all of the experimental devices were fully synchronized, enabling a very high level of reproducibility, each experiment was run twice under the exact same conditions. A first movie was recorded with the vertical vibration of the bath alone, then a second one followed, featuring both the vertical vibration and the signal wave. To obtain a better image of the signal wave and of its associated counter-propagating wave, the first movie was subtracted from the second one. This operation removes the boundary-induced ripples, which superpose exactly on the two movies. All of the following experimental movies were produced using this method.

Experimental Results and Discussion

We first study the response of the water-wave PCM to the signal wave from a point source in the configuration presented in Fig. 2 (Movie S1). Fig. 3A shows a snapshot of the wave field during the emission at $t \approx 0.43$ s. The signal wave is propagating outward and enters the deep end of the bath. This image appears similar to that of Fig. 2C, which is taken in the absence of a vertical excitation, because the PCM does not yet generate a phase-conjugated wave. In Fig. 3B, at $t \approx 1.44$ s, the source has stopped emitting and the PCM is emitting a phase-conjugated wave in the shallow end, that refocuses at the position of the source and diverges again on the other side of it. The signal wave has triggered the Faraday instability in the deep end and has imposed its shape as a boundary condition. In the absence of this perturbation, the surface of the deep end of the bath would remain flat since $t < \tau_F$. In the deep end, the Faraday instability is visible with standing waves at half the excitation frequency, with a shape that is given by the signal wave field and not by the boundaries of the basin. However, the boundary-induced ripples eventually take over, imposing the wave-field pattern in the deep end, as in standard stationary Faraday experiments. The shape of the propagating wave produced in the shallow end is thus lost. Fig. 3C shows the space-time plot along the horizontal x axis of Fig. 3A and B. It clearly shows that after the initial step, in which the wave source produces an outward-propagating field, a counterpropagating wave is produced in the deep end, resulting in the presence of symmetric wave fronts. These phase-conjugated waves are sustained even after the source has stopped emitting.

We now focus on the response of the PCM to various excitation frequencies. The wave profiles of the source are identical to the one described above, except for their frequency. The amplitude of the phase-conjugated wave is measured for each frequency through the light reflected on the surface reaching the camera, at the position of the source. Unfortunately, this measurement is not quantitative: The amplitude of the refocusing phase-conjugated waves can only be inferred qualitatively from the change in the reflection amplitude. The spectral response of the PCM is thus normalized by its maximum amplitude value obtained at the Faraday frequency. Fig. 3D shows the normalized spectral response of the PCM for three different bath accelerations, $\gamma_0/\gamma_F \approx 1, 1.35,$ and 1.6 . The shapes of the spectra are very similar with a sharp peak at the Faraday frequency, and the full width of the peak is approximately $\Delta f \approx 4$ Hz. This spectral response is independent of the excitation amplitude γ_0 of the vertical excitation of the bath. The sharp decrease of the PCM

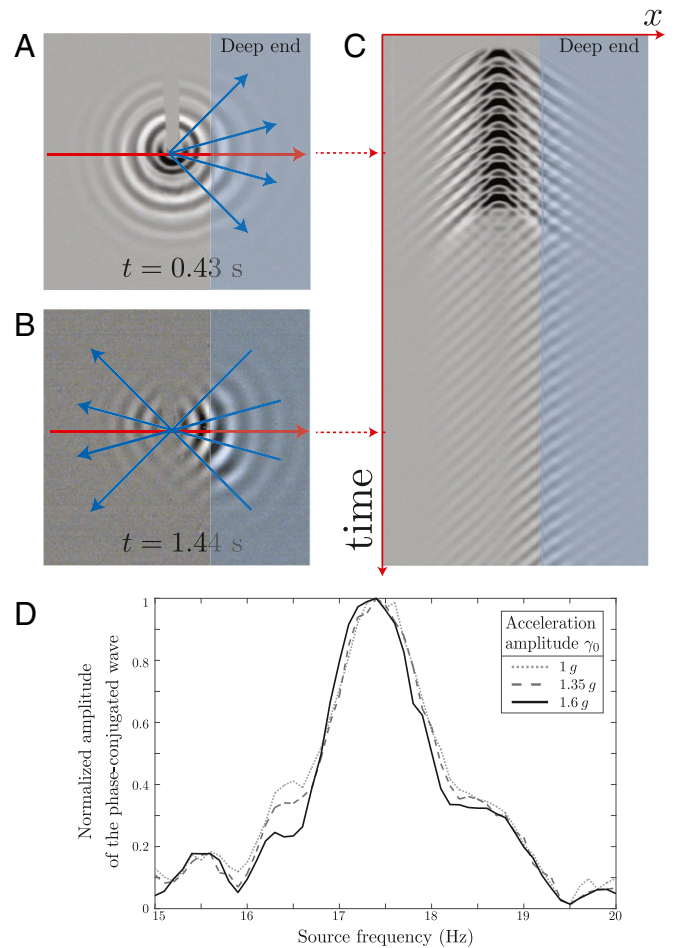


Fig. 3. Reflection of the signal wave emitted by a point source by a water-wave PCM based on the Faraday instability. The source and the bathymetry configurations are the ones presented in Fig. 2. The PCM is the deep end of the bath. Snapshots of the wave field: (A) during the source emission ($t \sim 0.43$ s), when the signal wave field enters the PCM, and (B) after the emission is turned off ($t \sim 1.44$ s), when the phase-conjugated wave refocuses at the source initial position (Movie S1). (C) Space-time plot associated to the image sequence along the solid red line in A and B. (D) Normalized spectral response of the water-wave PCM for various acceleration amplitudes γ_0 .

response when the source frequency deviates from the Faraday frequency is due to the phase mismatch between the incident wave and the phase-conjugated wave, due to a large dispersion in water. For $\Delta f \approx 4$ Hz, the coherence length is equal to ~ 5 Faraday wavelengths, which is already smaller than the width of the deep end (17). Although the phase-conjugated wave amplitude is not obtained qualitatively, the reflected light variations increase significantly with the acceleration amplitude: by a factor of 1.5 and 2.75 when the acceleration amplitude increases by 1.35 and 1.6, respectively. This is the signature of a strong increase in the efficiency of the PCM with increasing pumping. The theoretical dependence given by the model in Eq. 5 gives a linear dependence with the excitation amplitude.

Another classical configuration which exemplifies the difference between a standard mirror and a PCM is the case of an incident plane wave. Contrary to a standard mirror, for which the incident wave is reflected symmetrically to the normal of the mirror plane, a PCM produces waves which are phase-conjugated and counterpropagating. Fig. 4A and B shows two snapshots of a plane wave impinging toward a water-wave PCM and the resulting reflected phase-conjugated emission from the PCM (Movie S2).

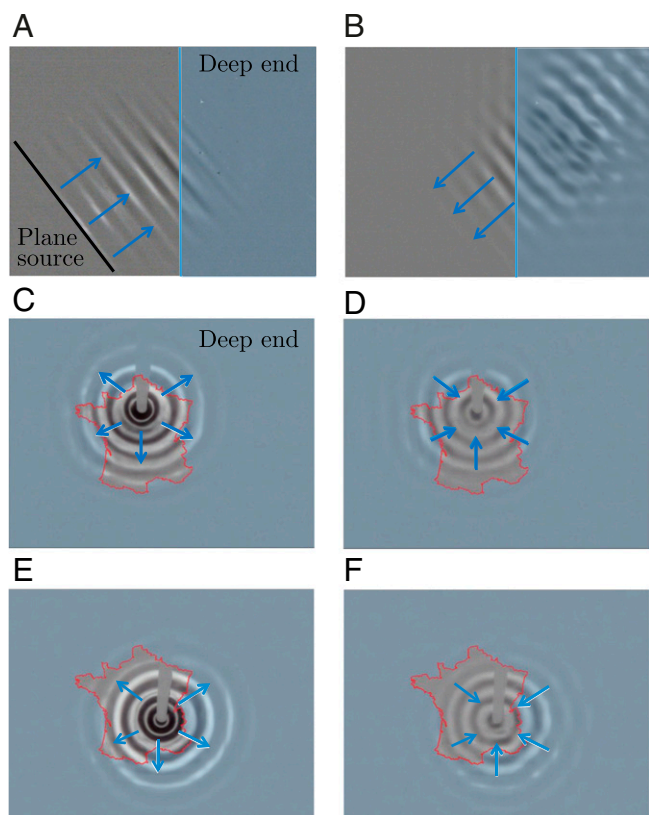


Fig. 4. Snapshots of various water-wave PCM configurations. (A and B) Snapshots of a plane wave impinging on a PCM ($t \sim 0.35$ s) and the reflected phase-conjugated counterpropagating wave generated by the PCM ($t \sim 1.1$ s), respectively (Movie S2). The bathymetry configuration is the one presented in Fig. 2. The PCM is the deep end of the bath. (C–F) Snapshots of a point-source emission placed at the position of Paris (C and D) and Lyon (E and F) surrounded by a water-wave PCM having the shape of France (see Movies S3 and S4, respectively). The PCM associated with the deep end of the bath is situated outside France, while the shallow end, inside France, corresponds to free wave propagation. The sources are similar to the one presented in Fig. 2. (C and E) are taken during source emission ($t \sim 0.3$ s) and (D and F) are taken when the source has stopped emitting, while the PCM is generating the phase-conjugated wave ($t \sim 1.13$ s).

The time profile of the source is the same as that of Fig. 2D. Fig. 3A shows the wave field during the emission at time $t \approx 0.35$ s and Fig. 3B when the source has stopped emitting, at $t \approx 1.1$ s. The triggered Faraday instability is clearly visible in the deep end as well as the counterpropagating phase-conjugated wave emitted in the shallow end.

The ability of PCMs to generate phase-conjugated waves is independent of their shape because there are no phase-matching conditions involved. Unlike standard mirrors, they can assume any shape. We have tested this unique property in an experiment in which the mirror is shaped like France, as shown in Fig. 4C–F. The shallow end of the bath is located within the borders of the country. It is surrounded by a deeper bath acting as a PCM for water waves when excited parametrically. Fig. 4C and E show the circular outward-propagating waves emitted by point sources, placed respectively at the location of Paris and Lyon ($t \approx 0.3$ s). Fig. 4D and F shows the phase-conjugated waves produced by the PCM surrounding France after the emission has stopped ($t \approx 1.13$ s). The waves refocus at the position of Paris and Lyon, respectively, and diverge again, producing standing waves centered at the initial source locations (see Movies S3 and S4, respectively).

It is interesting to relate water-wave PCMs using the Faraday instability to the recently introduced general concept of the instantaneous time mirror (ITM) (18). A water-wave ITM consists of submitting a liquid bath to a single sudden change of effective gravity. It results in the production of a broad-band, counter-propagating, time-reversed wave for any propagating wave initially present on the surface. This transient parametric excitation corresponds to a change in the wave-propagation speed on the entire surface of the bath. The water-wave PCM using the Faraday instability corresponds to a periodic modulation of the wave-propagation speed at the excitation frequency. Thus, PCMs can be analyzed as the monochromatic counterparts of ITMs.

PCMs based on the Faraday instability offer a unique way to see in real time the dynamics of the phase-conjugated generation directly inside the PCM material. This generation appears very efficient compared with other PCMs, like in optics for instance. It is the result of a temporal modulation of the speed velocity at the Faraday frequency. In the case of water waves, the wave-speed modulation can reach values on the order of the speed without modulation c_0 . With acceleration amplitudes satisfying $\gamma_0 \ll \omega_{exc}^2/k$, the wave speed satisfies $c(t) \approx c_0 + (\gamma_0/2\omega_{exc})\cos(\omega_{exc}t)$. Hence, in this experiment the wave-speed modulation is substantial. This is in sharp contrast with the typical values for optical PCMs, for which the wave modulation is very small, even for very large amplitudes of the pump beams (pulsed beams must be used to increase the efficiency of these types of PCMs). Indeed, typical values of the third-order susceptibility are in the range $\chi^{(3)} \approx 10^{-24}$ m²/V².

The phase-conjugated mode is generated immediately as the source wave enters the deep end of the bath. Each spatial wave front generates periodically at the Faraday frequency a copropagating wave, which adds up coherently with the incident wave, and a counterpropagating wave, which refocuses on the source. As the wave propagates into the deep end, the produced waves add up constructively from each propagating wave front, increasing the forward-propagating mode and the phase-conjugated mode. Following Eq. 5, the amplitude of the phase-conjugated mode increases with the acceleration modulation. The right-hand side of the equation represents the sources which produce this mode. There is no discontinuity in the phenomenon due to the Faraday instability threshold. However, above the Faraday threshold, ripples produced by the boundaries of the deep end of the bath will eventually get amplified. The characteristic time involved, τ_F , is long since the sources which produce it are initially null (right-hand side of Eq. 5). The growth rate is the result of the competition between the modulation of the vertical acceleration and the damping rate (which in turn is fixed by viscosity and boundary conditions). Self-oscillations can also be reached in optical FWM configurations but usually for crystal thicknesses much larger than the light wavelength (13, 19).

The efficiency of Faraday-based PCMs opens up the possibility of creating thin subwavelength PCMs, that could be used for time-reversed flat lenses (20), whose implementation is still very challenging with other types of waves (21, 22).

This paper revisits the Faraday instability as a way to control the propagation of water waves. This parametric instability is based on a modulation of the effective gravity, which induces a wave-velocity modulation. Equivalently, several others parametric instabilities using modulated electric or magnetic fields could be performed on fluids to induce similar modulations of the wave velocity (23–25). They could thus be revisited as well, being interpreted as PCMs to control wave propagation. These parametric controls appear much more versatile than the gravity modulation of the Faraday instability, in particular regarding the ability to perform differentiated control in different areas of the medium. In addition, the bathymetry technique used in this paper to confine the PCM to a particular area of the bath has the drawback of increasing the damping in the shallow region. This

limits the wave-propagation length, and can be avoided with these other parametric controls, enabling exciting experiments with a longer propagation length, like the control of focusing and propagation in complex media (26).

1. Faraday M (1831) On a peculiar class of acoustical figures; and on certain forms assumed by groups of particles upon vibrating elastic surfaces. *Philos Trans R Soc London* 121:299–340.
2. Benjamin TB, Ursell FJ (1954) The stability of the plane free surface of a liquid in vertical periodic motion. *Proc R Soc Lond A Math Phys Sci* 225:505–515.
3. Douady S (1990) Experimental-study of the Faraday instability. *J Fluid Mech* 221:383–409.
4. Kumar K, Tuckerman LS (1994) Parametric instability of the interface between two fluids. *J Fluid Mech* 279:49–68.
5. Westra MT, Binks DJ, van de Water W (2003) Patterns of Faraday waves. *J Fluid Mech* 496:1–32.
6. Domino L, Tarpin M, Patinet S, Eddi A (2016) Faraday wave lattice as an elastic metamaterial. *Phys Rev E* 93:050202.
7. Kumar S (2000) Mechanism for the faraday instability in viscous liquids. *Phys Rev E Stat Phys Plasmas Fluids Relat Interdiscip Topics* 62:1416–1419.
8. Cerda EA, Tirapegui EL (1998) Faraday's instability in viscous fluid. *J Fluid Mech* 368:195–228.
9. Douady S, Fauve S (1988) Pattern selection in Faraday instability. *Europhys Lett* 6:221–226.
10. Tsai SC, Tsai CS (2013) Linear theory on temporal instability of megahertz faraday waves for monodisperse microdroplet ejection. *IEEE Trans Ultrason Ferroelectr Freq Control* 60:1746–1755.
11. Tsai SC, Lin SK, Mao RW, Tsai CS (2012) Ejection of uniform micrometer-sized droplets from Faraday waves on a millimeter-sized water drop. *Phys Rev Lett* 108:154501.
12. Hellwarth RW (1977) Generation of time-reversed wave fronts by nonlinear refraction. *J Opt Soc Am* 67:1–3.
13. Yariv A, Pepper DM (1977) Amplified reflection, phase conjugation, and oscillation in degenerate four-wave mixing. *Opt Lett* 1:16.
14. Born M, Wolf E (1959) *Principles of Optics* (Cambridge Univ Press, Cambridge, UK).
15. Pietschmann D, Stannarius R, Wagner C, John T (2013) Faraday waves under time-reversed excitation. *Phys Rev Lett* 110:094503.
16. Eddi A, Fort E, Moisy F, Couder Y (2009) Unpredictable tunneling of a classical wave-particle association. *Phys Rev Lett* 102:240401.
17. Saleh BEA, Teich MC (2007) *Nonlinear optics. Fundamentals of Photonics* (John Wiley & Sons, Ltd., Hoboken, NJ), 2nd Ed., pp 737–798.
18. Bacot V, Labousse M, Eddi A, Fink M, Fort E (2016) Time reversal and holography with spacetime transformations. *Nat Phys* 12:972–977.
19. Bloom DM, Liao PF, Economou NP (1978) Observation of amplified reflection by degenerate four-wave mixing in atomic sodium vapor. *Opt Lett* 2:58.
20. Pendry JB (2008) Time reversal and negative refraction. *Science* 322:71–73.
21. Palomba S, et al. (2011) Optical negative refraction by four-wave mixing in thin metallic nanostructures. *Nat Mater* 11:34–38.
22. Harutyunyan H, Beams R, Novotny L (2013) Controllable optical negative refraction and phase conjugation in graphite thin films. *Nat Phys* 9:423–425.
23. Nevolin VG (1983) Parametric excitation of oscillations of a fluid flowing out of a container. *Fluid Dynam* 18:293–295.
24. Robinson JA, Bergougnou MA, Castle GSP, Incelet II (2001) The electric field at a water surface stressed by an AC voltage. *IEEE Trans Ind Appl* 37:735–742.
25. Briskman VA, Shaidurov GF (1969) Parametric excitation of fluid instability in magnetic and electric fields. *Magnetohydrodynamics* 5:10–12.
26. Lerosey G, de Rosny J, Tourin A, Fink M (2007) Focusing beyond the diffraction limit with far-field time reversal. *Science* 315:1120–1122.

ACKNOWLEDGMENTS. We thank Yves Couder, Matthieu Labousse, and Sander Wildeman for insightful discussions. The authors acknowledge the support of the AXA Research Fund and of the French National Research Agency (ANR) through LabEx WIFI (Laboratoire d'Excellence Waves and Imaging from Fundamentals to Innovation) (ANR-10-LABX-24).